Available online at www.sciencedirect.com
ScienceDirect
Journal of Molecular Catalysis A: Chemical 283 (2008) 5–14
JOURNAL OF MOLECULAR CATALYSIS A: CHEMICAL
www.elsevier.com/locate/molcata

Vanadyl acetylacetonate anchored onto amine-functionalised clays and catalytic activity in the epoxidation of geraniol

Clara Pereira [a], Ana Rosa Silva [a], Ana Paula Carvalho [b], João Pires [b,*], Cristina Freire [a,**]

[a] *REQUIMTE, Departamento de Química, Faculdade de Ciências, Universidade do Porto, R. Campo Alegre, 4169-007 Porto, Portugal*
[b] *Departamento de Química e Bioquímica, Centro de Química e Bioquímica, Faculdade de Ciências, Universidade de Lisboa, Campo Grande Ed. C8, 1749-016 Lisboa, Portugal*

Received 12 May 2007; received in revised form 19 November 2007; accepted 23 November 2007
Available online 5 December 2007

Abstract

The parent clays laponite (Lap) and K10-montmorillonite (K10) and those functionalised with (3-aminopropyl)triethoxysilane (APTES) were used as supports to immobilise vanadyl(IV) acetylacetonate ([VO(acac)$_2$]). All the materials were characterised by elemental analysis, XRD, TG-DSC, nitrogen adsorption isotherms at −196 °C and IR spectroscopy. The K10-based materials were also characterised by XPS.

In the case of K10-based materials, higher vanadium content was obtained for the APTES-functionalised K10, showing that the clay functionalisation enhanced the complex anchorage. In Lap-based materials the opposite tendency was observed, with a higher vanadium loading being obtained for direct complex immobilisation onto the parent clay. This is probably due to clay particles aggregation (resultant from the delaminated nature of Lap) provoked by functionalisation with APTES. Furthermore, FTIR data pointed out that in the amine-functionalised clays, the VO(IV) complex was anchored by Schiff condensation between the carbonyl groups of the acetylacetonate ligand and the amine groups from the grafted APTES, whereas the direct immobilisation of the complex onto the parents clays took place mostly through covalent bonding between the metal centre and the clay surface hydroxyl groups.

The [VO(acac)$_2$]-based materials were tested in the epoxidation of geraniol using *t*-BuOOH as oxygen source and reused several times repeatedly. The [VO(acac)$_2$]APTES@K10 material was the most efficient and stable catalyst upon reuse (5 cycles), among the four materials tested, with a substrate conversion and 2,3-epoxygeraniol regioselectivity comparable to the homogeneous phase reaction; the organofunctionalisation of K10 was also quite advantageous in the catalytic reaction since it passivated some active sites of the K10 support. In the case of Lap-based materials, the [VO(acac)$_2$]@Lap was more catalytically efficient than [VO(acac)$_2$]APTES@Lap.

Keywords: Oxovanadium(IV) acetylacetonate; Laponite; Montmorillonite; Organosilane functionalisation; Allylic epoxidation

1. Introduction

Vanadyl(IV) acetylacetonate has been extensively used in the homogeneous epoxidation of allylic alcohols using *tert*-butylhydroperoxide (*t*-BuOOH) as oxygen source, showing to be a highly active, stereo- and regioselective catalyst [1–6]. This catalytic reaction is of great importance in organic synthesis since epoxides are versatile and highly valuable intermediates in the synthesis of natural products and biologically active substances [2,7,8]. Particularly, the epoxidation of geraniol catalysed by the [VO(acac)$_2$]-*t*-BuOOH system is a very important example of the high regioselectivity of this complex for the allylic double bond [1,3,4].

In accordance with the green chemistry principles, the immobilisation of transition metal complexes with catalytic properties onto solid matrixes or organic polymers is an important research subject that has received much attention in recent years [9–11]. In fact, when immobilised metal complexes are used in heterogeneous catalytic reactions, besides their intrinsic chemo-

* Corresponding author. Tel.: +351 217500898; fax: +351217500088.
** Corresponding author. Tel.: +351 22040259; fax: +351 220402659.
E-mail addresses: jpsilva@fc.ul.pt (J. Pires), acfreire@fc.up.pt (C. Freire).

1381-1169/$ – see front matter © 2007 Elsevier B.V. All rights reserved.
doi:10.1016/j.molcata.2007.11.034

and enantioselectivity, they bring up several advantages into the catalytic reaction, namely the easy catalyst separation and reusability in subsequent cycles/reactions [9–11].

Several studies regarding the immobilisation of vanadyl(IV) acetylacetonate complex onto solid supports have been reported in the literature. This complex has been directly immobilised onto silica gel, mesoporous silicas and alumina [12–14] followed by subsequent calcination to produce metal dispersed catalysts. It has been anchored onto amine-functionalised activated carbon [15] by reaction between the C=O group of the acetylacetonate (acac) ligand and the free amine groups previously grafted onto the support surface. It has also been immobilised in polystyrene [16] by microencapsulation; in this case the complex is physically enveloped by a thin film of the polymer and is not covalently attached to the polymer matrix. The VO(IV) acetylacetonate anchored onto the functionalised activated carbon [15] and encapsulated in polystyrene [16] were used for the epoxidation of allylic alcohols, presenting similar catalytic activities to the homogeneous counterpart and could be reused without significant metal leaching.

Clays, either natural or modified, are important and versatile low-cost materials with a wide variety of applications namely in chemical industry, agriculture, surface coatings and environment purposes, as well as in catalysis as catalysts or catalyst supports [17,18]. Laponite (synthetic analogue of hectorite) and montmorillonite (natural smectite) are two smectite type clays that have been frequently used as supports for active catalysts [18]. Both laponite and montmorillonite present a 2:1 layer type structure formed by units constituted by one octahedral sheet sandwiched between two silica tetrahedral ones. The main difference between both clays is related with the octahedral layer composition: laponite is a trioctahedral clay with most of the octahedral sites occupied by Mg^{2+} ions, whereas montmorillonite is a dioctahedral clay with about two-thirds of the octahedral positions mainly occupied by Al^{3+} cations. Some partial metal cations substitution occurs in both clays, mainly in the octahedral layer, with Mg^{2+} being replaced by Li^{+} in laponite and Al^{3+} being replaced by Mg^{2+} and Fe^{2+}/Fe^{3+} in montmorillonite. The isomorphic substitutions create a net negative charge balanced by hydrated exchangeable cations (e.g. Na^{+}, Mg^{2+}, Ca^{2+}) in the interlayer space between adjacent 2:1 sheets [19–23].

In the present work, we attempt to functionalise laponite (Lap) and K10-montmorillonite (K10) with (3-aminopropyl) triethoxysilane (APTES) and use both organo-modified clays as supports for the vanadyl(IV) acetylacetonate catalyst. To evaluate the effectiveness of the complex anchoring onto the clays through the use of a spacer, the complex was also directly immobilised onto the parent clays. All the materials were characterised by elemental analysis, XRD, TG-DSC, nitrogen adsorption isotherms at −196 °C and FTIR; the K10-montmorillonite based materials were also analysed by XPS. Finally, the catalytic activity of the [$VO(acac)_2$]-based clay materials was studied at room temperature in the epoxidation of geraniol using *t*-BuOOH as oxygen source and their stability as heterogeneous catalysts after 5 catalytic cycles was correlated with the complex immobilisation procedure used in their preparation.

2. Experimental

2.1. Materials, reagents and solvents

K10-montmorillonite was supplied from Aldrich and laponite from Laporte Industries Ltd. Both solids were used as received. The compounds (3-aminopropyl)triethoxysilane, vanadyl(IV) acetylacetonate, chlorobenzene, geraniol and *tert*-butyl hydroperoxide solution 5.0–6.0 M in decane were obtained from Aldrich. Dichloromethane used in catalytic experiments was purchased from Romil (HPLC grade), chloroform was from Merck and dry toluene was from Aldrich.

2.2. Preparation of the materials

2.2.1. Functionalisation of the clays with (3-aminopropyl)triethoxysilane

Prior to use, the parent clays were heated in an oven to 120 °C for 1 h under vacuum. Afterwards, a mixture of clay (2.00 g) in dry toluene (100 cm^3) and 1.18 cm^3 of (3-aminopropyl)triethoxysilane (3-aminopropyl)triethoxysilane, APTES, (5.06 mmol) was refluxed for 24 h under argon atmosphere. The resulting material (APTES@Lap or APTES@K10) was filtered, refluxed with dry toluene (100 cm^3) for 2 h, and then dried in an oven at 120 °C under vacuum for 3 h (Scheme 1(a)).

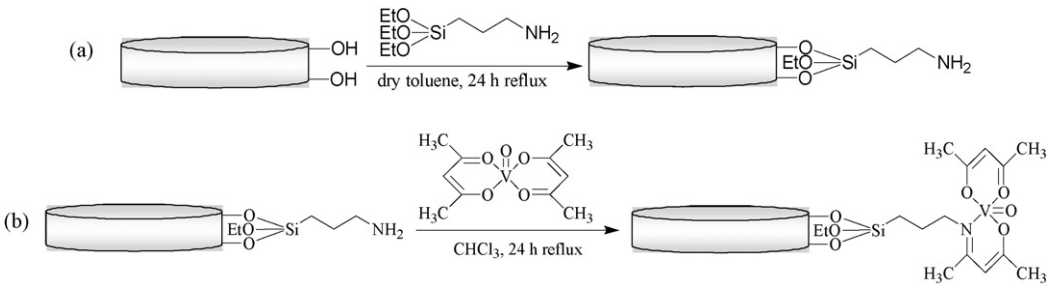

Scheme 1. Pathways on complex immobilisation onto organoclays: (a) functionalisation of the parent clays with (3-aminopropyl)triethoxysilane (APTES) and (b) anchoring of vanadyl(IV) acetylacetonate ([$VO(acac)_2$] onto APTES-functionalised clays.

2.2.2. Anchoring of vanadyl(IV) acetylacetonate onto APTES-functionalised clays

A solution of $[VO(acac)_2]$ (0.0239 g, 90 μmol) in chloroform (50 cm^3) was refluxed with APTES-functionalised clay (0.60 g) for 24 h. The resulting solids were filtered, refluxed with chloroform (50 cm^3) for 2 h, recovered by vacuum filtration and then dried in an oven to 120 °C for 3 h under vacuum (Scheme 1(b)). These materials will be referred to as $[VO(acac)_2]$APTES@Lap and $[VO(acac)_2]$APTES@K10.

2.2.3. Direct anchoring of vanadyl(IV) acetylacetonate onto clays

A solution of $[VO(acac)_2]$ (0.0239 g, 90 μmol) in chloroform (50 cm^3) was refluxed with clay (0.60 g) for 24 h. The resulting solids were filtered, refluxed with chloroform (50 cm^3) for 2 h, recovered by vacuum filtration and then dried in an oven to 120 °C for 3 h under vacuum. These materials will be labelled as $[VO(acac)_2]$@Lap and $[VO(acac)_2]$@K10.

2.3. Physico-chemical measurements

Vanadium contents were obtained by inductively coupled plasma emission spectrometry (ICP-AES), and nitrogen elemental analyses were performed at "Laboratório de Análises", IST, Lisboa (Portugal).

X-ray diffractograms were obtained with oriented mounts, on a Philips PX 1710 instrument using Cu Kα (λ = 1.5406 Å) graphite-monochromatised radiation. Thermogravimetric curves were obtained on a TG-DSC model 111 (Setaram, France), which had sensitivity of 10 μg. The experiments were made under a flux of dry nitrogen with a ramp of 2.5 °C/min between 25 and 650 °C. Nitrogen adsorption–desorption isotherms at −196 °C were measured on an automatic apparatus (ASAP 2010; Micromeritics). Before the adsorption experiments the samples were outgassed under vacuum for 2.5 h at 150 °C.

The FTIR spectra of the compounds were obtained with a Jasco FTIR-460 Plus spectrophotometer in the range 400–4000 cm^{-1}, using a resolution of 4 cm^{-1} and 32 scans. The spectra of the solids were obtained in KBr pellets (Merck, spectroscopic grade).

X-ray photoelectron spectroscopy (XPS) was performed at "Centro de Materiais da Universidade do Porto" (Portugal), on a VG Scientific ESCALAB 200A spectrometer using non-monochromatised Mg Kα radiation (1253.6 eV). The materials were compressed into pellets prior to the XPS studies. To correct possible deviations caused by electric charge of the samples, the C 1s band at 285.0 eV was taken as internal standard [24].

GC-FID chromatograms were obtained with a Varian CP-3380 gas chromatograph equipped with a FID detector, using helium as carrier gas and a fused silica Varian Chrompack capillary column CP-Sil 8 CB Low Bleed/MS (30 m × 0.25 mm i.d.; 0.25 μm film thickness). The conditions used for the epoxidation of geraniol were: 40 °C (3 min), 5 °C min^{-1}, 170 °C (2 min), 20 °C min^{-1}, 200 °C (15 min); injector temperature, 200 °C; detector temperature, 300 °C.

2.4. Catalysis experiments

The catalytic activity of the $[VO(acac)_2]$-based materials in the epoxidation of geraniol was studied at room temperature by using 1.00 mmol of geraniol (substrate), 0.50 mmol of chlorobenzene (GC internal standard) and 0.10 g of catalyst in 5.00 cm^3 of dichloromethane, under stirring conditions. The oxygen source, *t*-BuOOH (1.50 mmol), was progressively added to the reaction medium using a Bioblock Scientific Syringe Pump at a rate of 3.05 cm^3 h^{-1}. During the experiment, 0.05 cm^3 aliquots were taken from solution with a hypodermic syringe, filtered through 0.2 μm PTFE syringe filters and directly analysed by GC-FID. After reaction, the heterogeneous catalysts were separated from the reaction media by filtration and then refluxed/filtered with dichloromethane (50 cm^3) for 2 h, dried under vacuum in an oven to 120 °C for 2 h, and reused four times under the same experimental conditions as described above.

To provide a framework for the results obtained by using the heterogenised vanadyl(IV) complex, geraniol epoxidation was also carried out under experimental conditions comparable to

Table 1
Chemical analysis and textural properties (specific surface areas – A_{BET}, and mesoporous volumes – V_{meso}) of the clay-based materials

Sample	A_{BET} (m^2 g^{-1})	V_{meso}[a] (cm^3 g^{-1})	N[b] (mmol g^{-1})	V[c] (μmol g^{-1})
Lap	378	0.25		
APTES@Lap	145	0.09	0.9	
$[VO(acac)_2]$APTES@Lap	159	0.13		123
$[VO(acac)_2]$@Lap	346	0.21		130
K10	223	0.33		
APTES@K10	118	0.22	1.1 (1.12)[d]	
$[VO(acac)_2]$APTES@K10	112	0.21		132
$[VO(acac)_2]$@K10	212	0.32		53

[a] $V_{meso} = V_{total}(p/p0 = 0.97) - V_{micro}$ (from *t*-method).
[b] Nitrogen bulk content determined by elemental analysis (EA).
[c] Vanadium bulk content obtained by atomic emission spectroscopy (ICP-AES).
[d] mmol N/weight of sample (determined from XPS data in Table 2) = atom% N/[atom% C × Ar(C) + atom% N × Ar(N) + atom% O × Ar(O) + atom% Mg × Ar(Mg) + atom% Al × Ar(Al) + atom% Si × Ar(Si) + atom% K × Ar(K) + atom% Fe × Ar(Fe) + atom% Na × Ar(Na)].

those described above in (a) homogeneous media using the same amounts of $[VO(acac)_2]$ and (b) using the parent and APTES-functionalised clays without any added complex.

3. Results and discussion

The vanadyl(IV) acetylacetonate complex was immobilised onto the surface of the two clays, laponite and K10-montmorillonite, through the spacer APTES using the methodology depicted in Scheme 1. It is a two-step method that involves the previous functionalisation of the clays with APTES, and the subsequent reaction between the clay anchored amine groups and the carbonyl groups of the acetylacetonate ligand. To evaluate the effectiveness of this method, the complex was also directly anchored onto the unmodified clays.

3.1. Composition and textural characterisation

The nitrogen and vanadium elemental bulk contents of the clay-based materials are presented in Table 1.

The nitrogen loadings of the APTES-functionalised clays are 0.9 mmol g^{-1} for APTES@Lap and 1.1 mmol g^{-1} for APTES@K10, corresponding to functionalisation efficiencies (amount of grafted APTES/amount used in the reaction × 100) of 36 and 44%, respectively. Therefore, K10 presents a slightly higher content of grafted APTES than Lap. A possible explanation for this difference can be related to the differences in crystallite sizes, which are expected to be in the range of μm for K10, but much smaller for Lap, which has crystallite sizes in the range of nm [25]. In this way, the intercalation of APTES in the K10 clay layers can occur, a fact already reported in the literature [26], and therefore the retention of higher amounts of APTES in K10 can result from the reaction with OH from structural defects, not only at the edges but also in the layers.

The X-ray diffractograms for the Lap-based materials could not be obtained due to the low crystallite size and the delaminated nature of this material, a situation previously mentioned in the literature [25,27–29]. The diffractograms of the parent K10 and of APTES@K10 are presented in Fig. 1. The diffraction pattern for K10 is as expected for this type of material, presenting a d_{001} basal spacing of 0.9 nm. In the case of APTES@K10, in addition to the diffraction peak at $2\theta \approx 8.9°$, a broad peak centred at 2θ around 4.8° ($d = 1.79$ nm) is also noticed. This result can be attributed to the clay swelling due to the intercalation of APTES between the layers. Additionally, and as discussed elsewhere [26], the latter gallery height indicates a parallel-bilayer arrangement of APTES species.

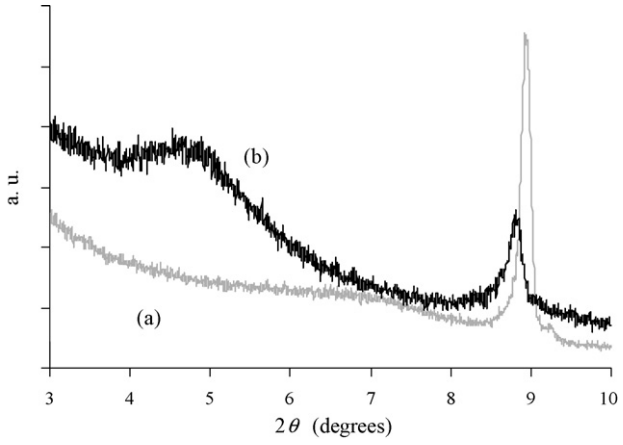

Fig. 1. X-ray diffractograms for: (a) K10 and (b) APTES@K10.

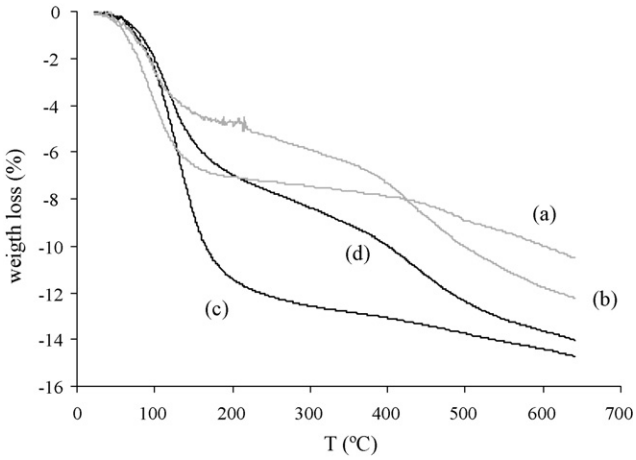

Fig. 2. Thermogravimetric curves for: (a) K10; (b) APTES@K10; (c) Lap; and (d) APTES@Lap.

The thermogravimetric curves for the samples with and without APTES are given in Fig. 2. The curves for K10 and Lap (curves (a and c), respectively) present a significant weight loss (more notorious for Lap) when the samples are heated until 200 °C, which is usually interpreted as the loss of adsorbed and bound water [19].

For temperatures higher than 200 °C, the Lap sample presents a weight loss with an almost continuous slope, while the weight of K10 remains fairly constant until about 450 °C, after which the slope increases, due to the dehydroxilation of the structure [19,23]. This difference may be a consequence not only of the different chemical composition of Lap and K10, but also of the different crystallite sizes, since it is known that a decrease in particle size may be accompanied by a decrease in the temperatures at which similar transformations occur [23].

In the curves for APTES@K10 and APTES@Lap ((b and d) of Fig. 2, respectively), the initial weight losses (below 200 °C) are lower than those observed for the parent materials, which is an indication that the amount of water in the clays was reduced after the reaction with APTES. Above 200 °C, the curves become almost parallel for both samples and the slopes are higher than for the initial K10 and Lap, showing that the APTES species decomposes over a wide range of temperatures. From the thermogravimetric curves for APTES@K10 and APTES@Lap an estimation of the amount of grafted APTES can be made; this estimation is based on the assumption that the APTES species decomposes into SiO_2, NH_3 and C_3H_6, as previously discussed in the literature [30]. From the weight losses between 200 and 600 °C, the nitrogen contents are estimated at 1.1 and 1.2 mmol g^{-1} for APTES@K10 and APTES@Lap, respectively. These values are in the range of those obtained by

chemical analysis (cf. Table 1), but due to the assumptions made in the calculations from the TG data, we consider the values from chemical analysis more reliable, and these will be used in the following work.

The vanadium bulk contents for [VO(acac)$_2$]APTES@Lap and [VO(acac)$_2$]APTES@K10 are 123 and 132 μmol g^{-1}, respectively, which correspond to total anchoring efficiencies (amount of adsorbed complex/amount in original solution × 100) of 82 and 88%. The APTES@K10 anchors only slightly higher quantities of [VO(acac)$_2$] than APTES@Lap, albeit its higher APTES content. This can be checked by the estimation of the anchoring efficiencies relative to the NH_2-surface contents, which are 14% for [VO(acac)$_2$]APTES@Lap and 12% for [VO(acac)$_2$]APTES@K10. The direct immobilisation efficiencies of [VO(acac)$_2$] onto the parent clays are 87% for [VO(acac)$_2$]@Lap and 35% for [VO(acac)$_2$]@K10. These results suggest that direct anchoring cannot be excluded in the case of functionalised clays (especially for laponite), although it must be highly reduced by the presence of the free amine groups at the clays surface.

The K10 functionalisation greatly enhances the anchorage of the VO complex in this clay, whereas for the Lap-based materials, higher V loading was obtained by direct complex immobilisation. This tendency was also observed for the immobilisation of a Mn(III)*salen* complex onto the parent and APTES-functionalised laponite [31].

Albeit there is no direct evidence for the fact that in Lap the highest amount of linked complex is obtained by direct immobilisation, the data of nitrogen adsorption isotherms at −196 °C can bring some clarification to this point. The nitrogen isotherms are given in Fig. 3(A and B) for the Lap- and the K10-based materials, respectively, and the corresponding values of specific surface areas (A_{BET}) and mesoporous volumes are listed in Table 1.

No significant microporosity (less than 0.05 cm^3 g^{-1}) is detected in the various materials by the *t*-method [32]. Therefore, the specific surface area and mesoporous volume of the materials in this work results essentially from the outer surface of the crystallites and from their aggregation. As can be seen in Fig. 3, all the isotherms present hysteresis loops as a consequence of the mesoporous nature of the samples. In the case of Lap materials, the initial sample (Fig. 3(A)(a)) presents the highest value of A_{BET} of the series (378 m^2 g^{-1}) but, when Lap is reacted with APTES (Fig. 3(A)(b)), the resulting material (APTES@Lap) has the lowest A_{BET} value of the Lap-based materials; that is, a decrease of 62% from the initial specific surface area is noticed.

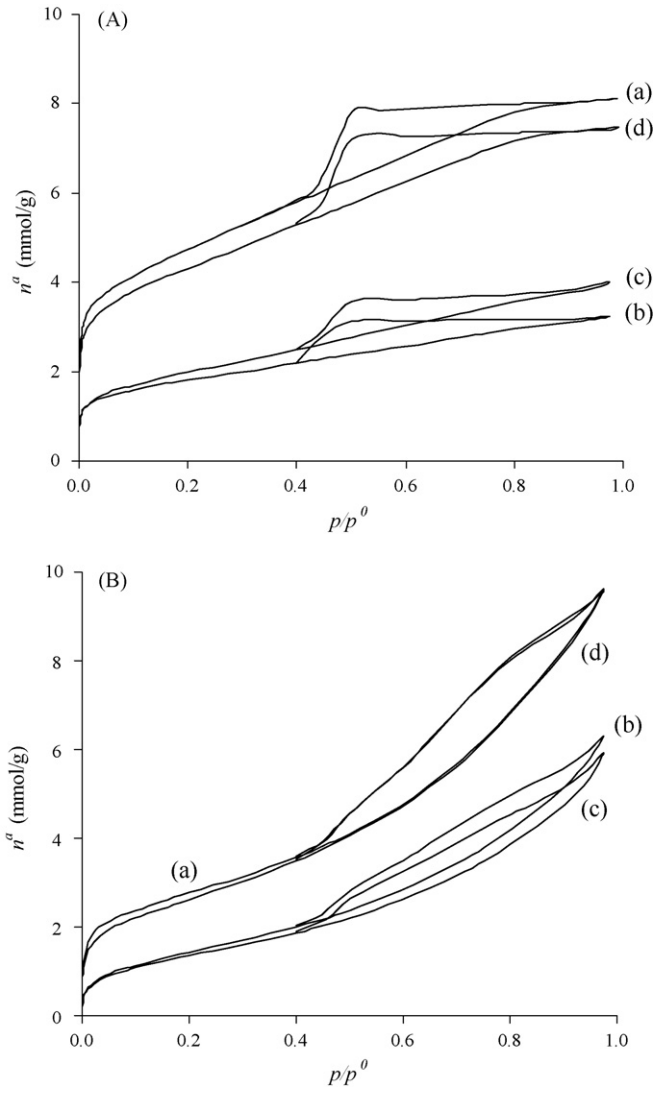

Fig. 3. Nitrogen adsoption–desorption isotherms at −196 °C. Panel (A) in the Lap-based materials: (a) Lap; (b) APTES@Lap; (c) [VO(acac)$_2$]APTES@Lap; and (d) [VO(acac)$_2$]@Lap. Panel (B) in the K10-based materials: (a) K10; (b) APTES@K10; (c) [VO(acac)$_2$]APTES@K10; and (d) [VO(acac)$_2$]@K10.

In the case of the K10 materials, grafting APTES (Fig. 3(B)(b)) results in a smaller decrease in A_{BET} to 47% from the initial value (Fig. 3(B)(a)). Apparently, the reaction with APTES promotes the aggregation of the clay particles, resulting in a decrease in the surface area. Due to the low aspect ratio of the Lap particles

Table 2
XPS atomic percentages for K10-based materials

Sample	Atomic%									
	C	N	O	Mg	Al	Si	K	Fe	Na	V
K10	5.14	0.32	58.51	1.25	5.04	29.11	0.22	0.42	—	—
APTES@K10	12.45	2.18	51.87	4.56	3.89	24.36	0.32	0.30	0.05	—
[VO(acac)$_2$]APTES@K10	13.83	2.33	50.73	2.06	4.37	25.88	0.19	0.38	0.21[a]	
[VO(acac)$_2$]@K10	7.02	0.30	56.37	1.60	5.73	28.23	0.33	0.38	0.05[a]	

Determined by the area of the respective XPS band in the high-resolution spectra.

[a] The vanadium surface content could not be determined as the V 2p$_{3/2}$ peak is overlapped with the O 1s satellite peaks; hence, the atomic percentages for the other elements were determined neglecting the vanadium atomic content.

and their related delaminated nature [29], the aggregation due to APTES had a more significant impact on the textural properties of the Lap materials.

Upon anchoring vanadium complex into the APTES-functionalised clays (curve (c) of Fig. 3(A and B)), different behaviour is observed. For the K10-based material there is a further, although slight, decrease in the A_{BET}, but for the Lap-based one the surface area increases, as a, as a consequence of an augment in crystallite disaggregation promoted by the anchoring of the complex. At this point it should be emphasised that the samples corresponding to direct immobilisation of the complex (curve (d) of Fig. 3(A and B)) retain the highest amount of the initial specific surface area for both Lap- and K10-based materials, which is significantly higher for the former material, as can be seen in Table 1. Therefore, in our view, the clear reduction in the available surface area for anchoring the complex, due to particle–particle aggregation that is registered for Lap treated with APTES, is the main reason why the complex loading obtained by this methodology is lower for this material than that obtained from direct anchoring. The fact that the amounts of complex loaded from direct immobilisation are higher for Lap than for K10 can also be justified by the higher surface area of this material compared to K10 (378 and 223 $m^2\,g^{-1}$, respectively). The related increased availability of crystallite edges and corresponding terminal OH groups in Lap can thus favour the anchoring of the complex.

The modified K10-based materials were also characterised by XPS. In Table 2 are summarised the XPS atomic percentages for K10-based materials and in Table 3 the results from curve fitting for the different regions; the XPS nitrogen surface content is included in Table 1. The bands due to the [VO(acac)$_2$] complex in the V 2p$_{3/2}$ region could not be clearly observed as they are partially masked by O 1s satellite peaks; therefore, no values could be obtained for the vanadium surface content and binding energy of the V 2p$_{3/2}$ band of the oxovanadium(IV) K10-based materials.

All the K10 materials present oxygen, silicon, aluminium and small amounts of magnesium, iron and potassium from the clay lattice. The high-resolution XPS spectrum of the parent clay shows a band at 103.3 eV in the Si 2p region assigned to silicon from the clay tetrahedral layers [33], a symmetrical band in the O 1s region at 532.6 eV due to single bonded oxygen from the clay lattice, a band centred at 74.9 eV due to Al^{3+} cations of the octahedral sheets and two bands, one at 1303.9 eV and other complex asymmetric band centred at 712.8 eV corresponding to magnesium and iron cations, respectively, from isomorphic substitution of Al^{3+} within the octahedral sheets. Low intensity and broad bands in the C 1s and N 1s regions are also observed and result from the presence of inorganic impurities within the clay.

Upon K10 functionalisation with APTES, there is a substantial increase in the carbon and nitrogen surface contents and a decrease in the oxygen content (Table 2). Furthermore, the peaks in the O 1s, C 1s and Si 2p regions show shifts to lower binding energy (BE) values and a new peak at 399.7 eV in the N 1s region is also observed, which can

Table 3
Curve fitting data of the XPS Spectra in the C 1s, O 1s, N 1s, Mg 1s, Si 2p, Al 2p, Fe 2p$_{3/2}$, K 2p$_{3/2}$ and Na 1s regions of the K10-based materials

Sample	Binding energy (eV)[a]									
	C 1s	O 1s	N 1s	Mg 1s	Si 2p	Al 2p	Fe 2p$_{3/2}$	K 2p$_{3/2}$	Na 1s	V 2p$_{3/2}$
K10	285.0 (2.6), 287.3 (3.0)	532.6 (2.6)	401.9 (5.4)	1303.9 (2.7)	103.3 (2.5)	74.9 (2.3)	712.8 (5.4)	293.5 (1.7)		
APTES@K10	285.0 (2.6), 286.3 (3.2)	532.2 (2.7)	399.7 (2.8), 402.1 (2.6)	1303.9 (2.6)	103.0 (2.6)	74.6 (2.3)	711.9 (6.7)	293.2 (2.3)	1072.3 (4.1)	
[VO(acac)$_2$]APTES@K10	285.0 (2.8), 287.0 (3.0)	532.1 (2.7)	399.8 (2.7), 402.0 (2.4)	1303.6 (2.5)	102.8 (2.5)	74.6 (2.3)	711.7 (5.9)	293.1 (1.9)	1073.4 (4.8)	[b]
[VO(acac)$_2$]@K10	285.0 (2.6), 286.8 (2.6)	532.5 (2.7)	401.4 (4.9)	1303.9 (2.6)	103.3 (2.5)	75.0 (2.4)	712.8 (5.4)	293.5 (1.9)	1072.7 (3.1)	[b]

[a] Values between brackets refer to the FWHM (full-width at half maximum) of the bands.
[b] The bands due to the [VO(acac)$_2$] complexes could not be observed in the V 2p$_{3/2}$ region as they were masked by the O 1s satellite peaks.

be assigned to the nitrogen from the APTES amine groups (Table 3). These results confirm the grafting of APTES onto the clays surface by reaction between the ethoxyl groups of APTES and surface hydroxyl groups catalysed by the clay adsorbed water; this reaction induces some hydrophobicity within the clay, as confirmed by TG and IR (see below). Additionally, a decrease in the binding energies of Fe $2p_{3/2}$, Al 2p and K $2p_{3/2}$ peaks is also observed, especially for Fe $2p_{3/2}$ peak, suggesting that the APTES linking agent reacts with hydroxyl groups present within the tetrahedral and octahedral sheets.

The nitrogen bulk and surface loadings, determined by EA and XPS, respectively (Table 1), are similar, indicating that APTES is homogeneously distributed throughout the clay matrix.

Upon anchoring the VO complex onto APTES@K10 and onto the parent clay, there is an increase in the atomic% of carbon and a decrease in the atomic% of oxygen, besides some disparate small changes in the atomic percentage of the other elements; furthermore, no significant changes were observed in the BE values of the different elements. These results, combined with the absence of the BE value of V $2p_{3/2}$, cannot be used to discriminate the different complex anchoring mechanisms that could be operative in both materials.

3.2. FTIR spectra

The FTIR spectra of the Lap and K10 clays are presented in Fig. 4. They exhibit two components associated with the OH stretching vibrations: in the case of Lap, a peak at approximately 3684 cm^{-1} corresponding to Mg–OH stretching vibration and a shoulder near 3626 cm^{-1} associated with Si–OH stretching vibration can be observed [22], whereas the spectrum of K10 exhibits a band at 3623 cm^{-1}, with a shoulder at about 3692 cm^{-1}, due to stretching vibrations of OH groups coordinated to octahedral cations (mainly Al, but also Mg and Fe) [20,21,34]. In both spectra, two bands related to the presence of interlayer H_2O (physisorbed water) are also observed: a broad band centred at 3457 cm^{-1} for Lap and 3435 cm^{-1} for K10 associated with OH stretching vibration and a band at 1643 cm^{-1} for Lap and 1632 cm^{-1} for K10, related to OH deformation [20–22,34,35].

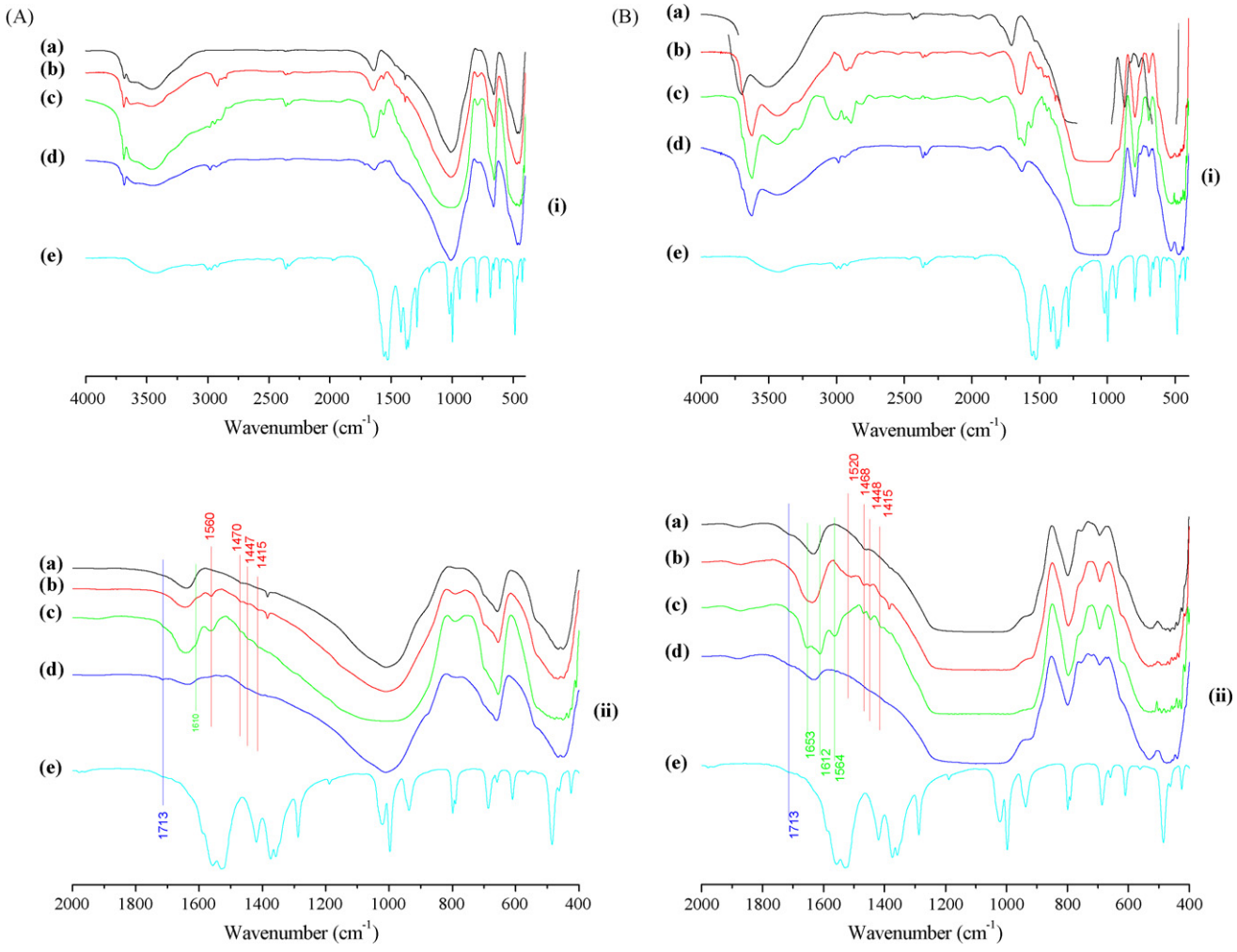

Fig. 4. FTIR spectra in the ranges (i) 4000–400 cm^{-1} and (ii) 2000–400 cm^{-1} of: (A) [VO(acac)$_2$] Lap-based materials (a) Lap, (b) APTES@Lap, (c) [VO(acac)$_2$]APTES@Lap, (d) [VO(acac)$_2$]@Lap and (e) [VO(acac)$_2$]; and (B) [VO(acac)$_2$] K10-based materials (a) K10, (b) APTES@K10, (c) [VO(acac)$_2$]APTES@K10, (d) [VO(acac)$_2$]@K10 and (e) [VO(acac)$_2$].

The Lap spectrum is also characterised by a broad and intense band centred at 1010 cm^{-1} assigned to Si–O stretching vibrations [36], one band at 658 cm^{-1} due to O–H bending of adsorbed water and an intense peak at about 450 cm^{-1} assigned to Si–O bending. In the K10 spectrum, besides the most intense band due to Si–O stretching vibrations of the tetrahedral layer observed in the range of 1200–1000 cm^{-1}, there are also peaks at 528 cm^{-1} due to Si–O–Al (octahedral Al) and 463 cm^{-1} due to Si–O–Si bending vibrations [20,21,34,37]. In addition, there is a shoulder at about 917 cm^{-1} matching the bending modes of structural Al–OH–Al [20,21,34,35] and a peak at 798 cm^{-1}, which was assigned by Tyagi et al. [21], Kloprogge et al. [34] and Madejová et al. [37] to the presence of quartz admixture in the sample, whereas Fialips et al. [38] attributed it to Si–O–Si vibrations and Grim [23] to Al–O–Si vibrations.

After APTES grafting onto Lap and K10, several changes can be observed in all the frequency range in the spectra (Fig. 4). One of the most important changes in the spectra is the decrease in the intensity of the bands associated with the interlayer clay water in the high energy range 3700–3000 cm^{-1}, due to OH stretching vibrations, as well as those at 1643 cm^{-1} for Lap and 1632 cm^{-1} for K10, related to OH deformation. This is a consequence of the grafting reaction between the APTES and the M–OH clay surface groups catalysed by the interlayer water, which induced some hydrophobicity within the clays (also detected by XPS and TG data). This effect leads to an apparent increase in the intensity of the peaks due to M–OH at 3684 cm^{-1} for Lap and 3623 cm^{-1} for K10, which are less accessible to the grafting reaction. The new NH_2 stretching band could not be resolved, due to being overlapped with the broad OH stretching band.

In the ranges of 2960–2850 cm^{-1} and 1470–1415 cm^{-1}, new bands from grafted APTES appear, corresponding to CH_2 stretching and bending vibrations, respectively; a band at 1560 cm^{-1} for Lap and a low intense broad band at 1520 cm^{-1} for K10, due to NH_2 bending vibrations, can also be observed [39–43]. The peak due to C–N stretching vibration and those of Si–CH_2–R, usually observed in the ranges 1200–1000 cm and 1250–1200 cm, respectively, could not be observed in either material as they were masked by the strong Si–O–Si stretching band [43].

The FTIR spectra of [VO(acac)$_2$]APTES@K10 and [VO(acac)$_2$]APTES@Lap show small changes in the ranges of 3700–3000 cm^{-1} and 1700–1200 cm^{-1}, compared to the parent materials, a consequence of the low complex content compared to that of APTES. In the OH stretching vibration region, the [VO(acac)$_2$]APTES@Lap spectrum shows an increase in intensity of the broad band centred at 3457 cm^{-1}, suggesting the presence of hydrogen bonds between the pseudo-π system of the acac ligand and the protons of the clay silanol groups [12–14], which apparently will not be so operative in the case of [VO(acac)$_2$]APTES@K10, since its spectrum does not show such a band intensity increase.

In the range of aliphatic C–H stretching vibrations (2900–2700 cm^{-1}) no significant changes are detected, even though VO complex vibrations are expected to occur at the same frequency region [44].

In the region of 1700–1400 cm^{-1} the changes are more perceptible in K10 due to the higher complex content. Nevertheless both materials show unaltered bands due to the grafted APTES at 1415, 1445, 1470 cm^{-1} (CH_2 bendings). In the K10-based material, a decrease in the intensity of the band at 1520 cm^{-1} (NH_2 stretching) and new bands at 1653, 1612 and 1564 cm^{-1} are clearly observed. For Lap-based material, a new band at 1610 cm^{-1} is only detectable, but the increase in intensity and broadness of the band centred at 1640 cm^{-1} (physically adsorbed water) suggests the presence of new bands with similar frequencies. These new bands have different frequencies from those of free [VO(acac)$_2$] [45], which is a first indication that a change in the coordination sphere of the complex took place. Some proofs for the latter assumption can be gathered by considering that the new bands at approximately 1653, 1612 and 1564 cm^{-1} in the spectrum of [VO(acac)$_2$]APTES@K10 may be due to combination vibration modes that include the stretching vibrations of the new C=N introduced in the chelate ring of the acac ligand by the anchoring reaction, the Schiff condensation reaction between the amine groups of the grafted APTES and the C=O group from the coordinated acetylacetonate ligand. Actually, a Mg-phyllosilicate sequentially functionalised with APTES and the acac ligand showed a band at 1608 cm^{-1} which was assigned to ν(C=N), following the fact that copper complexation showed a shift to approximately 1633 cm^{-1} [46].

The spectra of [VO(acac)$_2$]@K10 and [VO(acac)$_2$]@Lap are difficult to interpret since in the typical region for the complex bands, 1700–1400 cm^{-1}, there is a very intense band due to O–Si–O vibrations, which prevents any reliable comparison with the free complex bands. It is worth mentioning the presence of a new band at approximately 1710 cm^{-1}, for both materials, in a region typical for C=O stretching vibrations and in the high frequency region a decrease in the intensity of the broad band centred at 3457 cm^{-1} for [VO(acac)$_2$]@Lap and 3435 cm^{-1} for [VO(acac)$_2$]@K10. The latter observation renders evidence for the consumption of OH groups and can be taken as support for an immobilisation mechanism for [VO(acac)$_2$] by ligand exchange with the formation of a VO–O–clay bond, similarly to what is observed in the direct immobilisation of this complex in silica gel, mesoporous silica and alumina [13,14]. In this context the band observed at approximately 1710 cm^{-1} may be assigned to the de-coordinated acetylacetone ligand that is kept immobilised within the clays.

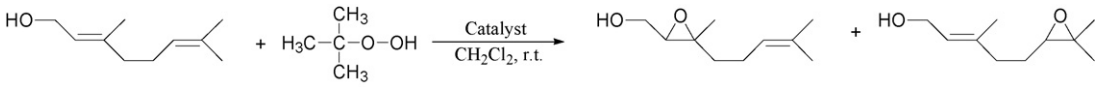

Scheme 2. Epoxidation of geraniol using *t*-BuOOH as oxygen source.

3.3. Catalytic epoxidation of geraniol

The [VO(acac)$_2$]-based materials were screened as heterogeneous catalysts in the epoxidation of geraniol, at room temperature, using *t*-BuOOH as oxygen source and dichloromethane as solvent (Scheme 2), and the results are summarised in Table 4; data from the homogeneous phase and the blank experiments (using the parent and amine-functionalised clays) run under similar conditions are also included.

All the [VO(acac)$_2$]-based materials catalyse the epoxidation of geraniol, with the geraniol conversion decreasing in the following order, for the 1st cycle: [VO(acac)$_2$]@K10 (100%) > [VO(acac)$_2$]@Lap (68%) > [VO(acac)$_2$]APTES@K10 (49%) > [VO(acac)$_2$]APTES@Lap (7%); yet, they show regioselectivity values towards the 2,3-epoxygeraniol (97–99%) comparable to those of homogeneous reactions. The required reaction times are longer than those for the homogeneous phase reactions, a common effect that is usually attributed to the diffusion constraints imposed on substrates and reactants by the porosity of the clay matrix [15] and in the case of the APTES based catalysts, the activity probably worsens by the change of the vanadium coordination sphere (O_4 to NO_3) caused by the anchoring procedure.

The recycling of all catalysts was tested for further 4 cycles and the vanadium bulk contents after the 5 cycles were determined. The following values are obtained, 80, 102, 79 and 9.8 μmol g^{-1}, for [VO(acac)$_2$]APTES@Lap, [VO(acac)$_2$]APTES@K10, [VO(acac)$_2$]@Lap and [VO(acac)$_2$]@K10, respectively, corresponding to leaching percentages of 35, 23, 39 and 81%.

It must be pointed out that upon catalyst recycling, the geraniol conversion increases for both the materials where the complex is anchored via APTES (although not so significantly for Lap-based material), whereas those in which the complex is directly immobilised show a decrease in the geraniol conversion. In this context, the [VO(acac)$_2$]APTES@K10 catalyst proves to be the most efficient and stable catalyst when reused (100% conversion after the 3rd cycle and 23% complex leaching after the 5th cycle, the lowest value among the four catalysts), affording a geraniol conversion and regioselectivity comparable to the homogeneous phase reaction. The [VO(acac)$_2$]@K10 catalyst shows a quite high leaching (the highest among the four materials), indicating that the high substrate conversion in the first 3 cycles might be due to the leached complex. Thus, for K10 materials, the anchoring procedure using APTES prevents leaching and deactivation of the active phase. On the other hand, both Lap-based catalysts show lower geraniol conversion than the homogeneous catalyst and have similar leaching percentages in the range of 35–39%. Hence, in the case of Lap-based materials the surface modification with APTES does not improve the catalytic activity of the immobilised complex.

The intrinsic catalytic activity of each support is low, except K10, confirming that the overall activity of the VO-based catalysts should be mainly due to the presence of the anchored complex. In fact, K10 clay itself is active in the oxidation of alcohols with *t*-BuOOH as oxygen source, as reported by Palombi et al. [47] due to the presence of reactive aluminium atoms in the octahedral layers and on sheets broken edges. Therefore, the high catalytic activity of [VO(acac)$_2$]@K10 in the first 3 cycles should be due to the support itself besides the contribution from the leached complex. Upon functionalisation with APTES, the support shows very low catalytic activity, suggesting that the spacer hinders the active sites of the parent clay, and therefore its contribution to the catalytic activity of [VO(acac)$_2$]APTES@K10 becomes minimal.

Combination of all results indicates that the grafting method through APTES leads to more chemically and catalytic stable material in the case of K10, but laponite proves to be a better support for direct anchoring of [VO(acac)$_2$].

Table 4
Epoxidation of geraniol, at room temperature, catalysed by [VO(acac)$_2$] in homogeneous and heterogeneous phase

Catalyst	Run	*t* (h)	% C[a]	% S[b]	
				2,3-EG	6,7-EG
[VO(acac)$_2$], 0.005 mmol[c]		0.5	100	99	1
[VO(acac)$_2$], 0.013 mmol[d]		0.5	100	99	1
[VO(acac)$_2$]APTES@Lap	1st	48	7	97	3
	2nd	48	26	98	2
	3rd	48	28	98	2
	4th	48	24	98	2
	5th	48	19	98	2
[VO(acac)$_2$]APTES@K10	1st	48	49	98	2
	2nd	48	99	98	2
	3rd	48	100	98	2
	4th	48	100	98	2
	5th	48	100	98	2
[VO(acac)$_2$]@Lap	1st	48	68	99	1
	2nd	48	56	99	1
	3rd	48	75	99	1
	4th	48	62	99	1
	5th	48	44	99	1
[VO(acac)$_2$]@K10	1st	48	100	98	2
	2nd	48	100	98	2
	3rd	48	100	98	2
	4th	48	30	94	6
	5th	48	23	94	6
Lap[e]		48	7	95	5
K10[e]		48	40	84	16
APTES@Lap[e]		48	11	97	3
APTES@K10[e]		48	6	95	5

Reaction conditions used: 1.00 mmol of geraniol, 0.50 mmol of chlorobenzene (internal standard), 0.10 g of heterogeneous catalyst, 1.50 mmol of *t*-BuOOH; solvent: dichloromethane.

[a] Based on geraniol consumption.

[b] Selectivity of the geraniol epoxide: 2,3-epoxygeraniol (2,3-EG) relative to 6,7-epoxygeraniol (6,7-EG).

[c] Homogeneous phase reaction using the same vanadium content as [VO(acac)$_2$]@K10.

[d] Homogeneous phase reaction using the same vanadium content as [VO(acac)$_2$]APTES@Lap, [VO(acac)$_2$]APTES@K10 and [VO(acac)$_2$]@Lap.

[e] Carried out under similar experimental conditions but with 0.10 g of supporting material.

4. Concluding remarks

Vanadyl(IV) acetylacetonate has been successfully immobilised onto the clays, laponite and K10-montmorillonite,

functionalised with APTES. The complex has also been directly anchored onto the two unmodified clays.

The amine-functionalisation of the two clays was more effective in the case of K10 probably caused by the larger crystallites size, which led to grafting not only in clay edges but also between the sheets.

The immobilisation of the VO complex onto the K10-based materials resulted in higher vanadium loading for APTES@K10, thus demonstrating that the organofunctionalisation of the clay improved the complex grafting. For Lap-based materials, the opposite tendency was observed, with higher vanadium content being obtained for direct complex immobilisation. This fact was probably due to the delaminated character of this material; APTES grafting induced the particles aggregation, preventing the anchoring of the complex to some extent. The immobilisation of vanadyl(IV) acetylacetonate onto the two APTES-functionalised clays proceeded mainly by Schiff condensation between the carbonyl group of the acetylacetonate ligand and the free amine groups previously grafted onto the clays surface; the direct complex immobilisation onto the parent clays occurred mostly through a covalent bond between the metal centre and the clays surface hydroxyl groups.

In geraniol epoxidation, the $[VO(acac)_2]$APTES@K10 material was the most efficient and stable catalyst when reused (5 cycles), with a substrate conversion and 2,3-epoxygeraniol regioselectivity comparable to the homogeneous phase reaction. In K10, the functionalisation with APTES was quite advantageous since it increased not only the amount of anchored complex, but also passivated some active sites of the K10 itself, which could have undesirable selectivity. In the case of Lap-based materials, the $[VO(acac)_2]$@Lap was more catalytically efficient than $[VO(acac)_2]$APTES@Lap.

Acknowledgments

This work was funded by FCT Fundação para a Ciência e a Tecnologia (FCT) and FEDER, through the project ref. POCI/CTM/56192/2004. CP thanks FCT for a PhD fellowship.

References

[1] V. Conte, F. Di Furia, G. Licini, Appl. Catal. A: General 157 (1997) 335–361.
[2] C. Bolm, Coord. Chem. Rev. 237 (2003) 245–256.
[3] A.G.J. Ligtenbarg, R. Hage, B.L. Feringa, Coord. Chem. Rev. 237 (2003) 89–101.
[4] K.B. Sharpless, R.C. Michaelson, J. Am. Chem. Soc. 95 (1973) 6136–6137.
[5] B.E. Rossiter, T.R. Verhoeven, K.B. Sharpless, Tetrahedron Lett. 20 (1979) 4733–4736.
[6] T. Itoh, K. Jitsukawa, K. Kaneda, S. Teranishi, J. Am. Chem. Soc. 101 (1979) 159–169.
[7] Q.-H. Xia, H.-Q. Ge, C.-P. Ye, Z.-M. Liu, K.-X. Su, Chem. Rev. 105 (2005) 1603–1662.
[8] W. Zhang, H. Yamamoto, J. Am. Chem. Soc. 129 (2007) 286–287.
[9] M.H. Valkenberg, W.F. Hölderich, Catal. Rev. 44 (2002) 321–374.
[10] A. Corma, H. Garcia, Adv. Synth. Catal. 348 (2006) 1391–1412.
[11] B.M.L. Dioos, I.F.J. Vankelecom, P.A. Jacobs, Adv. Synth. Catal. 348 (2006) 1413–1446.
[12] S. Shylesh, A.P. Singh, J. Catal. 244 (2006) 52–64.
[13] A.-M. Hanu, S. Liu, V. Meynen, P. Cool, E. Popovici, E.F. Vansant, Micropor. Mesopor. Mater. 95 (2006) 31–38.
[14] M. Baltes, O. Collart, P. Van der Voort, E.F. Vansant, Langmuir 15 (1999) 5841–5845.
[15] B. Jarrais, A.R. Silva, C. Freire, Eur. J. Inorg. Chem. (2005) 4582–4589.
[16] A. Lattanzi, N.E. Leadbeater, Org. Lett. 4 (2002) 1519–1521.
[17] H.H. Murray, Appl. Clay Sci. 17 (2000) 207–221.
[18] A. Vaccari, Appl. Clay Sci. 14 (1999) 161–198.
[19] B. Velde, Introduction to Clay Minerals, Chemistry, Origins, Uses and Environmental Significance, Chapman & Hall, London, 1992.
[20] J. Madejová, Vib. Spectrosc. 31 (2003) 1–10.
[21] B. Tyagi, C.D. Chudasama, R.V. Jasra, Spectrochim. Acta Part A 64 (2006) 273–278.
[22] N.N. Herrera, J.-M. Letoffe, J.-P. Reymond, E. Bourgeat-Lami, J. Mater. Chem. 15 (2005) 863–871.
[23] R.E. Grim, Clay Miner, McGraw-Hill, New York, 1968.
[24] J.F. Moulder, W.F. Stickle, P.E. Sobol, K.D. Bomben, in: J. Chastain (Ed.), Handbook of X-ray Photoelectron Spectroscopy, PerkinElmer, 1992.
[25] R.A. Schoonheydt, Introduction to zeolite science and practice, in: H. van Bekkum, E.M. Flanigen, J.C. Jansen (Eds.), Stud. Surf. Sci. Catal., 58, Elsevier, Amsterdam, 1991, p. 201.
[26] H. He, J. Duchet, J. Galy, J.-F. Gerard, J. Colloid Interface Sci. 288 (2005) 171–176.
[27] P. Cool, E.F. Vansant, Micropor. Mater. 6 (1996) 27–36.
[28] J. Pires, A. Carvalho, M.B. de Carvalho, Micropor. Mesopor. Mater. 43 (2001) 277–287.
[29] T.J. Pinnavaia, M.-S. Tzou, S.D. Landau, R.H. Raythatha, J. Mol. Catal. 27 (1984) 195–212.
[30] S.A. Alekseev, V.N. Zaitsev, Chem. Mater. 18 (2006) 1981–1987.
[31] I. Kuźniarska-Biernacka, A.R. Silva, A.P. Carvalho, J. Pires, C. Freire, Langmuir 21 (2005) 10825–10834.
[32] F. Rouquerol, J. Rouquerol, K. Sing, Adsorption by Powders & Porous Solids, Academic Press, San Diego, 1999.
[33] D. Zhao, Y. Yang, X. Guo, Inorg. Chem. 31 (1992) 4727–4732.
[34] J.T. Kloprogge, E. Mahmutagic, R.L. Frost, J. Colloid Interface Sci. 296 (2006) 640–646.
[35] A.M. Shanmugharaj, K.Y. Rhee, S.H. Ryu, J. Colloid Interface Sci. 298 (2006) 854–859.
[36] N.N. Herrera, J.-L. Putaux, E. Bourgeat-Lami, Prog. Solid State Chem. 34 (2006) 121–137.
[37] J. Madejová, J. Bujdák, M. Janek, P. Komadel, Spectrochim. Acta Part A 54 (1998) 1397–1406.
[38] C.-I. Fialips, S. Petit, A. Decarreau, D. Beaufort, Clays Clay Miner. 48 (2000) 173–184.
[39] K.A. Carrado, L. Xu, R. Csencsits, J.V. Muntean, Chem. Mater. 13 (2001) 3766–3773.
[40] D. Jiang, Q. Yang, J. Yang, L. Zhang, G. Zhu, W. Su, C. Li, Chem. Mater. 17 (2005) 6154–6160.
[41] Y. Liu, M. Wang, Z. Li, H. Liu, P. He, J. Li, Langmuir 21 (2005) 1618–1622.
[42] S. Tanaka, M. Tada, Y. Iwasawa, J. Catal. 245 (2007) 173–183.
[43] X. Wang, J.C.C. Chan, Y.-H. Tseng, S. Cheng, Micropor. Mesopor. Mater. 95 (2006) 57–65.
[44] K. Nakamoto, Infrared and Raman Spectra of Inorganic and Coordination Compounds, John Wiley & Sons, Inc., New York, 1997.
[45] P. Van der Voort, I.V. Babitch, P.J. Grobet, A.A. Verberckmoes, E.F. Vansant, J. Chem. Soc. Faraday Trans. 92 (1996) 3635–3642.
[46] I.L. Lagadic, Micropor. Mesopor. Mater. 95 (2006) 226–233.
[47] L. Palombi, F. Bonadies, A. Scettri, J. Mol. Catal. A: Chem. 140 (1999) 47–53.